Optimal instantaneous power dispatch in hybridised modular fuel cell systems

Noé Rivier, Pauline Kergus, Jérémi Regnier, Amine Jaafar, Christophe Turpin, Malik Tognan

Optimal instantaneous power dispatch in hybridised modular fuel cell systems

Noé Rivier[1], Pauline Kergus[1], Jérémi Regnier[1], Amine Jaafar[1], Christophe Turpin[1], Malik Tognan[2]

Abstract

This article tackles the control of a multi-module fuel cell system. It compares two power management strategies: equi-distribution, in which the power is homogeneously split between the fuel cell modules and optimal distribution, in which the power dispatch can be heterogeneous, meaning all degrees of freedom of the multi modular system are explored. The aim of this work is to quantify what can be achieved with these additional degrees of freedom. The results show that when the system modules are identical, optimal distribution outperforms equi-distribution in a very narrow power range that are never observed in automotive application, where a battery is included in the system. However, when the fuel cell modules have different performances, the optimal distribution strategy saves around 1% in hydrogen consumption compared with the equi-distribution strategy.

1 Introduction

The necessary energy transition in the mobility sector is increasing the interest in hydrogen technology. In particular, heavy-duty mobility, requiring long range and short recharging times, is looking for an alternative to battery-powered electric vehicles [1]. PEMFC-LT (Proton Exchange Membrane Fuel Cell Low Temperature) technology, hybridised with a battery to take advantage of braking phases, represents a promising avenue for decarbonising this sector. However, to be used on an industrial scale, PEMFC-LT technology needs to improve its durability and lower its inherent costs. One approach is to use modular Fuel Cell (FC) systems:the FC system is made

*This work is part of the ECH2 project, financed by the French Government as part of the France 2030 plan operated by ADEME. The consortium is composed of: ALSTOM Hydrogène SAS, Siemens Digital Industries Software, IFP Energies Nouvelles, Vitesco Techonologies, Institut de Mathématiques de Toulouse and LAPLACE.

*Corresponding autor : rivier@laplace.univ-tlse.fr

*[1] LAPLACE, Université de Toulouse, CNRS, INPT, UPS, Toulouse, France.

*[2] H2 Pulse, Toulouse, France

up of several low-power modules instead of a single high-power module. This architecture enables individual control of each module. Several power dispatching strategies using this degree of freedom have been proposed to minimise the hydrogen consumption of hybrid multi-modular systems.

In [2][3][4] hybrid multi-modular FC systems are considered with 5, 4 and 4 modules respectively. The power dispatch strategy is done sequentially in two steps. The power demand is first split between the battery and the FC system, then the power assigned to the FC system is distributed between the modules according to different strategies. These three studies define as optimisation criteria the minimisation of the hydrogen consumption of the multi-modular system, or the maximisation of the efficiency of the said system. Each of these studies proposes a power dispatch strategy that optimises this criterion, which they compare with two reference strategies: equi-distribution and Daisy-Chain (a strategy that consists in using the minimum number of FC modules to supply the required power while respecting an inrush order [5]). The results are similar: the optimal distribution is heterogeneous until the power to be supplied by the multi-modular system is equal to the sum of the optimal powers of the modules. The optimum power of a module is defined as the power at which the module achieves maximum energy efficiency. Beyond this point, the solution switches to a homogeneous distribution. Similar work is carried out in [6] on a two-module fuel cell system not hybridised, with similar results to those of [2], [4] and [3]. The form of the optimal power dispatch remains the same no matter the considered numbers of modules. Nevertheless, it is important to emphasize that these optimal solution corresponds to an optimisation problem where the power is only distributed between the modules. However, a battery is present in most of these systems and, more generally, FC systems designed for mobility need to be hybridised [7].

In this context, this works aims at quantifying the gains obtained by using the degrees of freedom of multi-modular systems when the battery is included in the optimisation problem. In addition, it is important to account for the ageing behaviour of the module: in [8] and [9], adaptive power dispatch strategies are proposed, integrating the evolution of the characteristics of the FC modules as they age. In [8], online identification is performed to constantly update the time-varying characteristics of the power sources. In [9] a power management strategy called a Daisy-Chain Rotary is proposed: the order in which modules are called is constantly updated to give priority to calling the least degraded module. Compared to a conventional Daisy-Chain (fixed call order) and an equi-distribution strategy, it allows an hydrogen consumption saving of 5 to 10%.

The aim of this work is to evaluate the gains made by using the degrees of freedom offered by hybridized modular FC systems, both in the case of similar modules and modules with different states of health. This article is organized as follows. Section 2 presents the models describing the system

under investigation. Section 3 details the optimisation problem and the power considered distribution strategies. Section 4 compares the optimal and equi-distribution strategies for identical modules, base on numerical simulations. Section 5 focuses on the impact of ageing on the results of both strategies.

2 Considered system

The system under consideration consists of 3 FC modules hybridised with a battery. It is described by 3 sub-models, a FC operation model, a FC ageing model and a battery operation model (Figure 1). The whole system is controlled by the power dispatch policy block. The details of the sub-models are given in the following subsections.

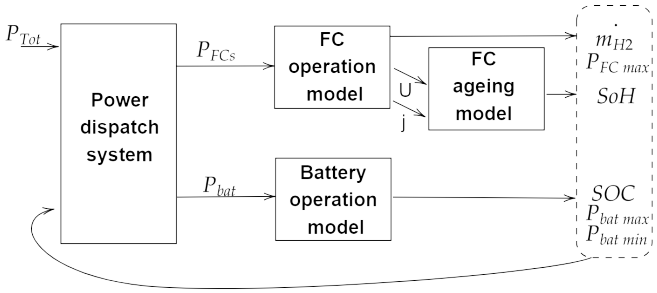

Figure 1: Architecture of the considered model: the required power (P_{tot}) is dispatched between the Fuel cell system (FCs) and the battery. From this distribution, the sub-models update the state variables and the state of health.

2.1 FC operation model

The model consists in a mapping of the performance of a FC stack given by a tabulation. For a given current density j and State of Health (SoH), defined by the FC ageing model, a table gives the net power output of the module (Figure 2).

Similarly, the hydrogen consumption of each module $\dot{m}_{iH_2}$ is tabulated (Figure 3). For a power demand, the module consumption increases as the SoH of the module deteriorates. The energy efficiency of a module is defined on the basis of its consumption $\dot{m}_{iH_2}$ [g/s], the lower heating value of the dihydrogen LHV_{H_2} [J/g] and its power P_i.

$$\eta_i = \frac{P_i}{\dot{m}_{i\ H_2} \cdot LHV_{H_2}} \tag{1}$$

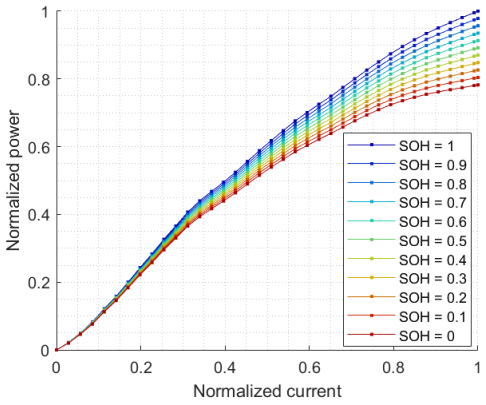

Figure 2: Module power curve as a function of current for different SoH

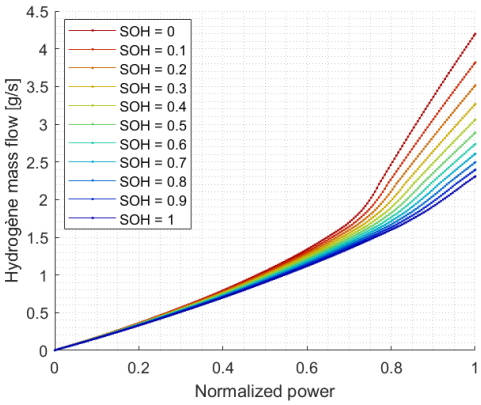

Figure 3: Module consumption curve as a function of power for different SoH

To account for the compressor's inertia, the model limits the modules power variations in the following way:

$$P_i^{max}(t+1) = P_i(\dot{m}_{air}^{max}(t+1)), \tag{2}$$

where the maximum air flow of the compressor $\dot{m}_{air}^{max}$ has limited variation given by:

$$\dot{m}_{air}^{max}(t+1) = \dot{m}_{air}(t) + \Delta\dot{m}_{air}^{max}, \tag{3}$$

where $\Delta\dot{m}_{air}^{max} = 0.0707\ [kg.s^{-2}]$.

2.2 FC ageing model

In this paper, the FC ageing model is based on the superposition principle as in [10] [11] [12]. It identifies specific degrading operating regimes and the corresponding decrease of the modules SoH. Four degrading regimes are considered:

- start degradation δ^{ss} [V]: if the i module switches from off to on $\delta_i^{ss} = \delta_{ref}^{ss}$, otherwise $\delta_i^{ss} = 0$.
- Open Circuit Voltage (OCV) δ^{OCV} [V]: when a module's voltage approaches its OCV, i.e. when $U > U^{\cdot}$,

$$\delta^{OCV} = k_{OCV}(U - U^{\cdot})^{n_{OCV}}$$

with $U^{\cdot} = 0.802[V]$. When $U <= U^{\cdot}$,

$$\delta^{OCV} = 0$$

- Operational degradation δ^j [V]: the degradation are proportionals to the current density within the FC cells:

$$\delta^j = k_j j$$

with j the current density in $[A.cm^{-2}]$.

- Power transition δ^{pt} [V]: only increases in power are counted, as the model assumes that a drop in the power supplied by a module does not cause any damage.

$$\delta^{pt} = k_{pt} \frac{j}{J_{lim}} \frac{\Delta j}{J_{lim} - \Delta j}^{n_{pt}}$$

Where Δj is the variation in current density over one second, $J_{lim} = 2.35$ $[A.cm^{-2}]$.

Table 1: Ageing model coefficients

Coefficient	δ^{ss}_{ref}	k_{OCV}	n_{OCV}	k_j	k_{pt}	n_{tp}
Value	2e-6	7.09e-7	2	2.49e-9	7.81e-6	2

The above coefficients (Table 1) have been adjusted based on a FC load derived from a Hyundai Nexo over a WLTC homologation cycle and an expected life of 10,000 hours at this load. This model and its parameters have not yet been experimentally validated.

Based on these 4 degradation regimes, the model calculates the instantaneous degradation $\delta^{tot}_i(t)$ of each module:

$$\delta^{tot}_i(t) = \delta^{ss}_i(t) + \delta^{OCV}_i(t) + \delta^j_i(t) + \delta^{tp}_i(t) \tag{4}$$

then the (SoH) variation of the modules $d_{SoH\ i}(t)$.

$$d_{SoH\ i}(t) = \frac{\delta^{tot}_i(t)}{\Delta V_{margin}} \tag{5}$$

Where ΔV_{margin} represents the maximum acceptable voltage drop to consider that a cell is still in working order and $\delta^{tot}_i(t)$ the total instantaneous degradation of the i module at time t. The SoH of modules is updated as follow:

$$SoH_i(t_k + 1) = SoH_i(t_k) + \int_{t_k}^{t_k+1} d_{SoH\ i}(t)dt \tag{6}$$

When a FC module is new, its SoH is equal to 1. When the SoH reaches 0, the module is considered to have reached the end of its life. Using the curve bundle in Figure 2, the ageing of modules is reflected in their performance during a simulation.

2.3 Battery operation model

The electrical performance of the battery is characterised by an internal resistance model from the Simcenter AMESim software. It is a model validated on experimental data [13]. The battery power and its voltage are given by:

$$\begin{cases} P_b = U_b \cdot I_b \\ U_b = U_{b\ ocv} - I_b \cdot R_b(SoC, P_b) \end{cases} \tag{7}$$

Where $U_{b\ ocv}$ is the open circuit voltage of the battery, I_b is the current flowing through the battery and $R_b(Soc, P_b)$ is its internal resistance varying with the state of charge (SoC) of the battery and the sign of P_b. In this work it is obtained from a tabulation. For a given battery power P_b and charge level SoC, I_b is calculated as follows:

$$I_b = \frac{U_{b\ ocv} - \sqrt{U_{b\ ocv}^2 - 4R_b(Soc, P_b)P_b}}{2R_b(Soc, P_b)} \tag{8}$$

From I_b the model estimates the variation in the battery's state of charge (d_{SoC}) using the following formula:

$$d_{SoC} = \frac{-I_b}{3600 \cdot Q_b} \tag{9}$$

Where Q_b represents the battery storage capacity. The SoC is updated as follow:

$$SoC(t_k + 1) = SoC(t_k) + \int_{t_k}^{t_k+1} d_{SoC}(t)dt \tag{10}$$

3 Power dispatch optimisation

The power dispatch is an equivalent consumption minimization strategy (ECMS) solving the following optimisation problem:

$$\begin{aligned} \min_{P_1,P_2,P_3,P_b} \quad & J(P_i, P_b) \\ \text{s.t.} \quad & P_1 + P_2 + P_3 + P_b = P_{tot} \\ & 0 \leq P_i \leq P_i^{max} \\ & P_b^{min} \leq P_b \leq P_b^{max} \end{aligned} \tag{11}$$

where P_{tot} is the total power to be supplied by the system, P_i the power supplied by module i and P_b the power supplied by the battery. The aim is

to minimise the hydrogen consumption of the multi-modular system. The following cost function is defined:

$$J = \underbrace{\sum_{i=1}^{3} k_{1i}(P_i)P_i}_{J_{H_2}} + \underbrace{k_2(SoC)P_b}_{J_{Bat}} \tag{12}$$

J_{H_2} represents the instantaneous hydrogen consumption of the multi-modular system.

$$\begin{cases} k_{1i}(P_i) = \frac{1}{\eta_i(P_i)} \\ J_{H_2} = \dot{m}_{H_2\ i} \cdot LHV_{H_2} \end{cases} \tag{13}$$

k_{1i} varies according to the power of the module i and its health level (Figure 4).

The second term, J_{Bat}, is used to penalise the use of the battery as a function of its SoC through the factor $k_2(SoC)$. When the battery SoC decreases, the value of $k_2(SoC)$ increases, penalising the use of the battery and vice-versa (Figure 5). The value of $k_2(SoC = 50\%)$ is defined as follows:

$$k_2(50\%) = min(k_{1i}(SoH = 0.8)) \tag{14}$$

It implies that when $SoC = 50\%$ it is just as interesting to use the battery as a module with a SoH of 0.8 at optimal power. The shape of k_2 is chosen so that the battery SoC remains around 50%. This is reflected in the steepness of the $k_2(SoC)$ curve around values of $SoC = 50\%$.

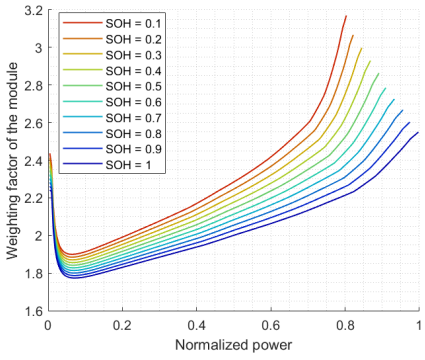

Figure 4: Evolution of k_1 as a function of module power supply for different SoH: the cost of using the modules increases as their SoH deteriorates.

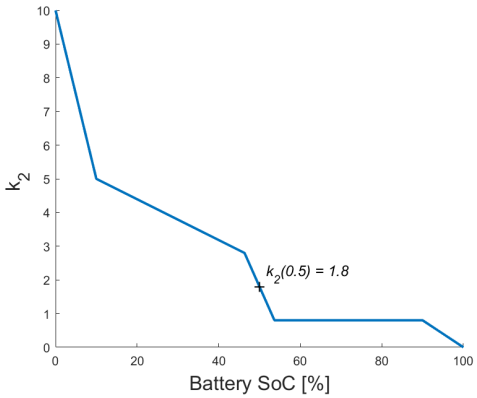

Figure 5: Evolution of k_2 as a function of the SoC. If the SoC is above 50%, $k_2 < k_1$, the battery is used instead of the modules.

3.1 Considered power management strategies

In order to assess the benefits of using the degrees of freedom of the multi-modular system, two power distribution strategies are considered.

3.1.1 optimal distribution with 3 degrees of freedom

$$\sum_{i=1}^{3} P_i = P_{FCs} \tag{15}$$

For a specific P_{tot} value, the search space is a three-dimensional space defined by (P_1, P_2,P_3). The value of P_b is restricted by the following equation when P_{tot} is given:

$$P_{FCs} + P_b = P_{tot} \tag{16}$$

3.1.2 equi-distribution with 1 degree of freedom

$$P_i = \frac{P_{FCs}}{3} \tag{17}$$

The modules powers P_i are identical. For a given value of P_{tot}, the search space is a one-dimensional space bounded by the constraint (16). It is important to note that the search space of the equi-distribution strategy is included in the search space of the optimal distribution strategy. Indeed, (17) acts as an additional constraint in the power dispatch problem (11).

3.2 Implementation

To solve the optimisation problem, the search space is divided into a mesh based on a power step. The algorithm calculates the value of J at every point in the mesh for a given value of P_{tot} and chooses the point that minimises J. The number of optimisation variables is impacted by the choice of power management strategy: three for optimal distribution and one for equi-distribution.

The time required to solve the optimization problem for the equi-distribution strategy is significantly less than that required for the optimal distribution strategy. For a given power step P_{step}, there are

$$N = \frac{P_{Fcs}^{max}}{P_{step}} \tag{18}$$

power combinations to be tested for the equi-distribution strategy. While there are N^3 possibilities for the equi-distribution strategy.

4 Power distribution in a hybrid multi-modular system with similar modules

In this section, we equi-distribution and optimal distribution are compared for FC modules with identical health levels.

4.1 Comparison with the literature

Various comparative studies of power allocation strategies in multi-modular FC systems are available in the literature. [2] [3] [4] [14] compare the equi-distribution strategy with optimal distribution strategies. It is essential to note that the system examined in these studies differs from our own. These studies focus exclusively on optimising the power distribution between FC modules, whereas our approach also integrates the battery in the process. The conclusions of these four studies show that there is an operating range for which optimal distribution is more advantageous than equi-distribution (shown in green on Figure 6).

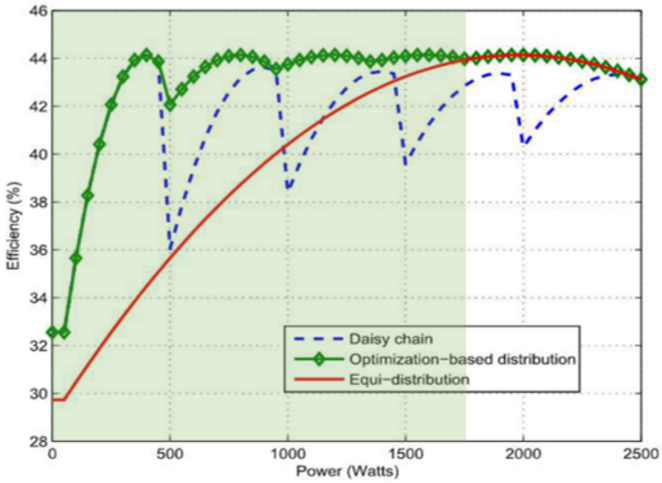

Figure 6: Energy efficiency of the multi-modular system in response to a power ramp for three distribution strategies [2]. The green area identifies the zone where heterogeneous distribution is more interesting than equal distribution.

For each value of SoH and P_{FCs}, the power distribution between the modules is determined by solving (11) in order to minimises the consumption of the multi-modular system. We identify two power ranges of the FC system for which a heterogeneous power distribution minimises the consumption of the multi-module system. These operating ranges are shown in green and grey in Figure 7 in a plane: normalized power of the FC system / SoH of

the modules.

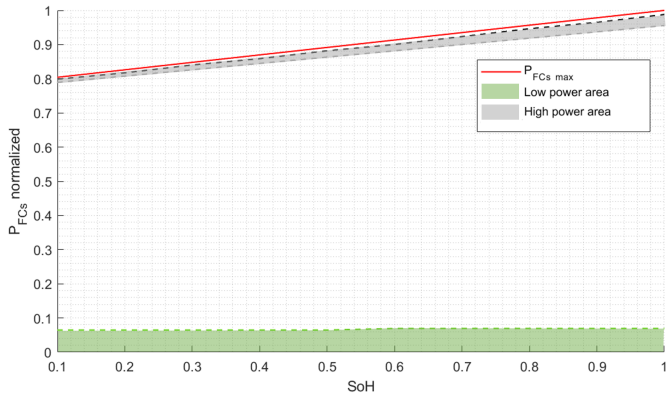

Figure 7: Multi-modular system power range where heterogeneous distribution is of interest.

The low-power zone was already described in [2] [3] [4] [14] (see Figure 6), it corresponds to the zone of increasing efficiency of the modules, delimited by $[0; P_{opt}(SoH)]$, where $P_{opt}(SoH)$ is the power at which the module reaches its maximum efficiency, for a given SoH. This zone is slightly increasing with SoH. It can be seen that this zone is more restricted than what appears in the literature. This can be explained by the difference between the efficiency curves of the FC modules of our model and the ones of [2] [3] [4] [14]. In our model, the optimum power of a module is achieved at a lower percentage of the maximum power (7%) than in [3] [4][2] (40%). When the systems operate in this low power range, it becomes more advantageous to use all degrees of freedom instead of relying on equi-distribution.

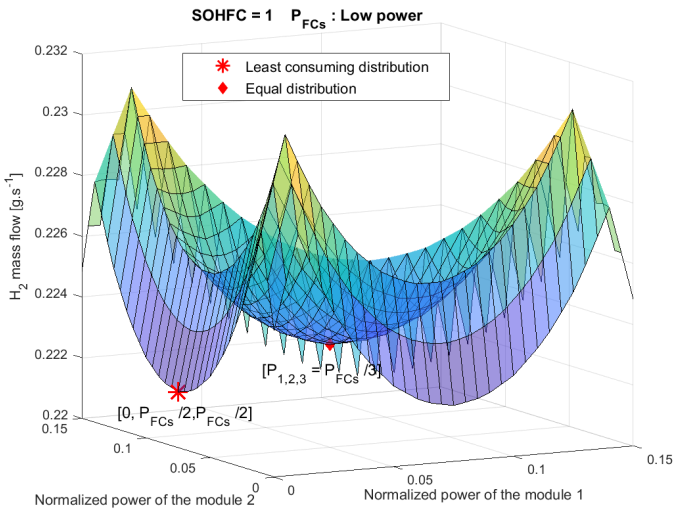

Figure 8: Consumption of the multi-modular system as a function of the power distribution between the modules for a P_{FCs} in the low power range.

To illustrate this point, Figure 8 represents the consumption of the multi-modular system as a function of the power distribution between the modules, for a power of P_{FCs} in the low power zone. It can be seen that the minimum consumption level is not reached for a homogeneous power distribution between the modules $(\frac{P_{FCs}}{3}, \frac{P_{FCs}}{3}, \frac{P_{FCs}}{3})$, but rather with a heterogeneous power distribution $(0, \frac{P_{FCs}}{2}, \frac{P_{FCs}}{2})$.

Figure 7 exhibits a very narrow high-power operating range, which is fairly close to the maximum power achievable by the multi-modular system. In this high-power zone, the distribution of power between the modules that minimises the consumption of the FC system is also heterogeneous.

4.2 Application to a heavy duty driving cycle

Two simulations are compared. The first is driven by the optimal distribution strategy and the second by the equi-distribution strategy. In both cases, the hybrid multi-modular system is subjected to the power profile of a 6-hour driving cycle (Figure 9).

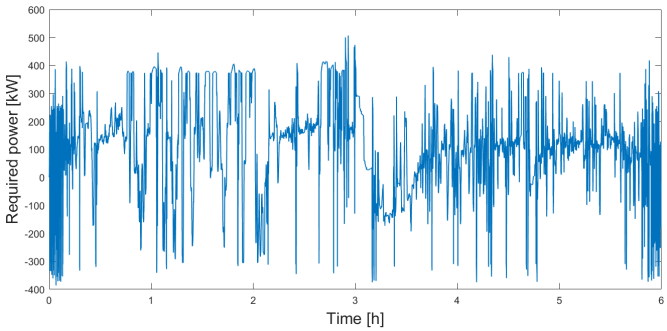

Figure 9: Full driving cycle power profile

By representing the power of the FC system at each instant of the simulation (Figure 10), it appears that the zones of heterogeneous power distribution identified in Figure 7 are never reached, therefore the power distribution over the entire driving cycle is the same for each of the strategies.

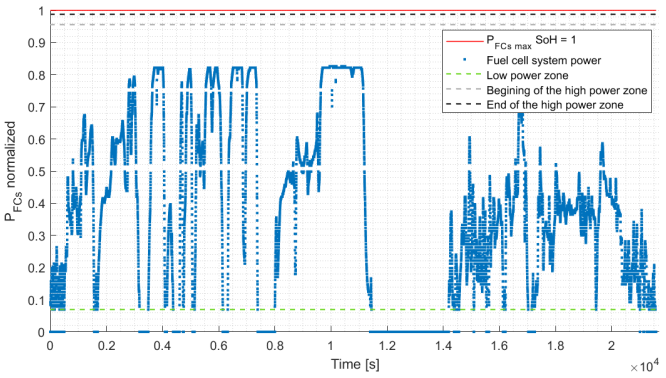

Figure 10: Power of the FC system for both strategies. The multi-modular system is not used in its operating ranges where the heterogeneous distribution would be optimal.

5 Power distribution in a hybrid multi-modular system with modules of different SoH

In practice, different modules are likely to perform differently, because of conception flaws or disparities, or premature ageing for instance. To place ourselves in this more realistic case, we now assume that the modules have different SoH and once again, the equi-distribution and optimal distribution strategies, solving (11), are compared. In both cases, the same power profile as before (Figure 9) is sent to the hybrid multi-modular system. The initial SoH of module 3 varies from 1 to 0.1, while the initial SoH of modules 1 and 2 is equal to 1.

5.1 Equivalent hydrogen consumption

In order to compare distribution strategies in terms of hydrogen consumption, it is necessary to include the battery's energy deficit or surplus in the simulation's hydrogen consumption despite different final SoC of the battery, as in[15] [11].

$$m_{H_2}^{tot} = m_{H_2}^{FC} + m_{H_2}^{bat} \tag{19}$$

$m_{H_2}^{FC}$ is obtained directly from the simulation. $m_{H_2}^{bat}$ must be estimated from the battery charge level at the end of the driving cycle. The energy surplus (or deficit) of the battery represents avoided (or additional) hydrogen consumption. The proposed conversion rate is the average H_2 consumption of the FC system per unit of energy produced by the FC system over the driving cycle. The modular system consumed $m_{H_2}^{FC}$ grams of H_2 for E_{FCs} Joules produced, so it has an average conversion rate of:

$$\tau = \frac{m_{H_2}^{FC}}{E_{FCs}}$$

τ in $g_{H_2}.J^{-1}$. It can therefore be argued that the energy surplus or deficit represents an hydrogen mass $m_{H_2}^{bat}$:

$$m_{H_2}^{bat} = E_{totbatterie}\Delta SoC\tau$$

5.2 Results

When the 3 modules have a similar initial SoH, we are in the same configuration as Section 4: both strategies dispatch the power homogeneously between the modules over the entire driving cycle. When the SoH of module 3 decrease, the optimal distribution strategy proposes a heterogeneous power distribution that spares the module with the lowest performance and requires a greater contribution from the other modules. The case $SoH_3^{ini} = 0.3$ is shown in Figure 11.

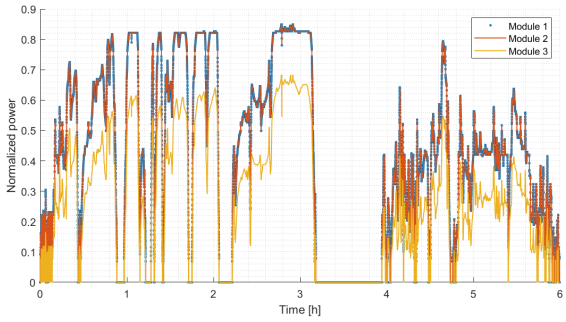

Figure 11: Power supplied by the FC modules over the driving cycle $SoH_3^{ini} = 0.3$: optimal distribution strategy

For each simulation, the final hydrogen consumption $m_{H_2}^{FC}$, the battery charge level at the end of the cycle SoC_{fin} and the corrected final consumption $m_{H_2}^{tot}$, see (19), are given in Table 2. The last line gives the gain in hydrogen consumption when using the optimal distribution strategy compared to equi-distribution. This value is calculated from the corrected consumption.

Table 2: Comparison of both strategies' hydrogen consumption

SOH_{ini} $m3$		1	0.9	0.8	0.7	0.6
$m_{H_2}^{FC}$ [g]	OD	43191	43354	43499	43632	43756
	Equi	43191	43359	43526	43691	43859
SoC_{fin}	OD	0.5027	0.5026	0.5024	0.5023	0.5022
	Equi	0.5027	0.5026	0.5024	0.5022	0.5020
$m_{H_2}^{tot}$ [g]	OD	43168	43333	43479	43612	43855
	Equi	43168	43337	43506	43672	43841
Gain %		0	0.01	0.06	0.14	0.24

SOH_{ini} $m3$		0.5	0.4	0.3	0.2	0.1
$m_{H_2}^{FC}$ [g]	OD	43873	43986	44094	44201	44304
	Equi	44033	44215	44401	44589	44782
SoC_{fin}	OD	0.5022	0.5021	0.5020	0.5020	0.5020
	Equi	0.5018	0.5017	0.5015	0.5013	0.5011
$m_{H_2}^{tot}$ [g]	OD	43855	43968	44077	44184	44287
	Equi	44017	44200	44388	44578	44773
Gain %		0.35	0.51	0.68	0.89	1.1

The consumption gain increases slightly as the initial health of module 3 deteriorates. At its maximum, the consumption gain achieved by the optimal distribution strategy is 1.1%, for an initial health of module 3 of 0.1.

Overall, optimal degradation degrades the modules slightly more than the equi-distribution. Performances of each simulation are summarised in Figure 12. For each SOH_3^{ini} value, the strategy that minimises a criterion (hydrogen consumption or ageing) is highlighted in green. The metric used to quantify ageing is the average drop in the SoH of each module over the course of the simulation:

$$J_{SoH} = \frac{1}{3}\sum_{i=1}^{3}(SoH_i^{ini} - SoH_i^{fin}). \tag{20}$$

Optimal distribution strategy generates more degradation related to start-up, see Figure 13a. This can be explained by the fact that the most degraded module is regularly stopped by the optimal distribution strategy. In addition, as the optimal distribution strategy places greater demands on

SOHini	mH2 (kg)		V_{loss}^{FC} (µV)	
	OD	Equi	OD	Equi
1	43.13	43.13	42.58	42.58
0.9	43.35	43.36	42.57	42.71
0.8	43.45	43.53	42.77	42.34
0.7	43.63	43.69	42.05	41.56
0.6	43.76	43.86	41.42	41.41
0.5	43.87	44.03	40.77	40.85
0.4	43.99	44.22	40.29	38.50
0.3	44.09	44.40	39.69	37.97
0.2	44.20	44.59	37.98	37.63
0.1	44.30	44.78	38.21	36.94

Figure 12: Consumption and ageing induced by the optimal distribution and equi-distribution strategy.

the two healthy modules, the amplitude of their power variations is greater. This can be seen in Figure 13b, which shows the degradation suffered by each of the modules in the two simulations of the case $SoH_3^{ini} = 0.3$. Conversely, the equi-distribution strategy causes more degradation due to the high voltage level of the cells (close to the OCV). The current density degradation is only slightly affected by the choice of power management strategy.

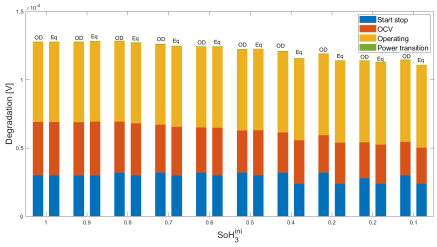

(a) Distribution of the average ageing of the 3 modules by degradation category for the two distribution strategies: optimal distribution (OD) / Equi-distribution (Eq)

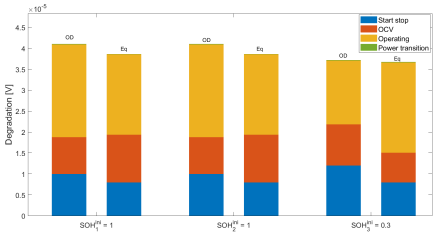

(b) Distribution of the ageing of the 3 modules in the simulations $SoH_3^{ini} = 0.3$ for the two distribution strategies. The power transition degradation are indistinguishable as they are hundred times lower than others degradation.

Figure 13: Impact of distribution strategy on module ageing.

6 Conclusions and outlooks

The results of this study mitigate the benefits of controlling the modules of a hybrid multi-modular system individually. When the modules are identi-

cal, the equi-distribution strategy is optimal. When the FC modules have different SoH, the optimal distribution strategy is optimal, but the H_2 gains made compared with an equi-distribution strategy are small, less than or equal to 1%.

The content of this article focuses only on instantaneous optimisation. The ECMS power distribution algorithm does not guarantee that the minimum energy consumption over the driving cycle has been achieved. It would therefore be interesting to use an optimal control strategy over the whole driving cycle and to evaluate the gains of using all degrees-of-freedom of multistack FC systems in this new strategy.

Acknowledgment

We would like to thank Paul Boucharel and Jérôme Lachaize of Vitesco Technologies for providing the model of the multi-modular FC system. This work is part of the ECH2 project, financed by the French Government as part of the France 2030 plan operated by ADEME. The consortium is composed of: ALSTOM Hydrogène SAS, Siemens Digital Industries Software, IFP Energies Nouvelles, Vitesco Techonologies, Institut de Mathématiques de Toulouse and LAPLACE.

References

[1] D.-Y. Lee, A. Elgowainy, A. Kotz, R. Vijayagopal, and J. Marcinkoski, "Life-cycle implications of hydrogen fuel cell electric vehicle technology for medium- and heavy-duty trucks," *Journal of Power Sources*, vol. 393, pp. 217–229, Jul. 2018, ISSN: 03787753. DOI: 10.1016/j.jpowsour.2018.05.012.

[2] J. E. Garcia, D. F. Herrera, L. Boulon, P. Sicard, and A. Hernandez, "Power sharing for efficiency optimisation into a multi fuel cell system," in *2014 IEEE 23rd International Symposium on Industrial Electronics (ISIE)*, Jun. 2014, pp. 218–223. DOI: 10.1109/ISIE.2014.6864614.

[3] N. Marx, D. C. Toquica Cárdenas, L. Boulon, F. Gustin, and D. Hissel, "Degraded mode operation of multi-stack fuel cell systems," *IET Electrical Systems in Transportation*, vol. 6, no. 1, pp. 3–11, 2016, ISSN: 2042-9746. DOI: 10.1049/iet-est.2015.0012.

[4] D. C. Toquica Cardenas, N. Marx, L. Boulon, F. Gustin, and D. Hissel, "Degraded Mode Operation of Multi-Stack Fuel Cell Systems," in *2014 IEEE Vehicle Power and Propulsion Conference (VPPC)*, Oct. 2014, pp. 1–6. DOI: 10.1109/VPPC.2014.7007041.

[5] A. Macias, M. Kandidayeni, L. Boulon, and H. Chaoui, "A novel online energy management strategy for multi fuel cell systems," in *2018 IEEE International Conference on Industrial Technology (ICIT)*, Feb. 2018, pp. 2043–2048. DOI: 10.1109/ICIT.2018.8352503.

[6] T. Wang, Q. Li, L. Yin, and W. Chen, "Hydrogen consumption minimization method based on the online identification for multi-stack PEMFCs system," *International Journal of Hydrogen Energy*, pp. 5074–5081, Feb. 26, 2019, ISSN: 0360-3199. DOI: 10.1016/j.ijhydene.2018.09.181.

[7] C. C. Chan, "The State of the Art of Electric, Hybrid, and Fuel Cell Vehicles," *Proceedings of the IEEE*, vol. 95, no. 4, pp. 704–718, Apr. 2007, ISSN: 0018-9219. DOI: 10.1109/JPROC.2007.892489.

[8] R. Ghaderi, M. Kandidayeni, M. Soleymani, L. Boulon, and J. P. F. Trovao, "Online Health-Conscious Energy Management Strategy for a Hybrid Multi-Stack Fuel Cell Vehicle Based on Game Theory," *IEEE Transactions on Vehicular Technology*, pp. 1–1, 2022, ISSN: 0018-9545, 1939-9359. DOI: 10.1109/TVT.2022.3167319.

[9] A. Macias Fernandez, M. Kandidayeni, L. Boulon, and H. Chaoui, "An Adaptive State Machine Based Energy Management Strategy for a Multi-Stack Fuel Cell Hybrid Electric Vehicle," *IEEE Transactions on Vehicular Technology*, vol. 69, no. 1, pp. 220–234, Jan. 2020, ISSN: 1939-9359. DOI: 10.1109/TVT.2019.2950558.

[10] J. M. Desantes, R. Novella, B. Pla, and M. Lopez-Juarez, "A modeling framework for predicting the effect of the operating conditions and component sizing on fuel cell degradation and performance for automotive applications," *Applied Energy*, vol. 317, p. 119 137, Jul. 1, 2022, ISSN: 0306-2619. DOI: 10.1016/j.apenergy.2022.119137. (visited on 11/02/2022).

[11] Z. Hu *et al.*, "Multi-objective energy management optimization and parameter sizing for proton exchange membrane hybrid fuel cell vehicles," *Energy Conversion and Management*, vol. 129, pp. 108–121, Dec. 1, 2016, ISSN: 0196-8904. DOI: 10.1016/j.enconman.2016.09.082.

[12] A. Pessot *et al.*, "Development of an aging estimation tool for a pem fuel cell submitted to a mission profile," *Fuel Cells*, vol. 20, no. 3, pp. 253–262, 2020.

[13] E. Prada, J. Bernard, R. Mingant, and V. Sauvant-Moynot, "Li-ion thermal issues and modeling in nominal and extreme operating conditions for HEV / PHEV's,"

[14] Y. Wang, W. Chen, A. Guo, and X. Shen, "Two-Level Energy Management Strategy for a Hybrid Power System Based Multi-Stack Fuel Cell," pp. 545–556, Feb. 8, 2022. DOI: 10.1061/9780784483886.058.

[15] Y. Liu, J. Liu, Y. Zhang, Y. Wu, Z. Chen, and M. Ye, "Rule learning based energy management strategy of fuel cell hybrid vehicles considering multi-objective optimization," *Energy*, vol. 207, p. 118 212, Sep. 15, 2020, ISSN: 0360-5442. DOI: 10.1016/j.energy.2020.118212.